Fuel 144 (2015) 400–414

Contents lists available at ScienceDirect

Fuel

journal homepage: www.elsevier.com/locate/fuel

A semi-analytical solution to optimize single-component solvent coinjection with steam during SAGD

Mohsen Keshavarz [1], Ryosuke Okuno *, Tayfun Babadagli

School of Mining and Petroleum Engineering, University of Alberta, Canada

HIGHLIGHTS

- An analytical method is presented for estimating oil drainage rates of coinjection.
- Three components are considered: oil, solvent, and water.
- The method is validated against numerical simulation results.
- Results show the importance of solvent accumulation near the chamber edge.
- Less volatile solvents tend to remain effective at lower operating pressures.

ARTICLE INFO

Article history:
Received 24 August 2014
Received in revised form 11 December 2014
Accepted 15 December 2014
Available online 24 December 2014

Keywords:
Steam-assisted gravity drainage
Bitumen recovery
Steam–solvent coinjection
Analytical solution
Phase behavior

ABSTRACT

Coinjection of a low concentration of solvent with steam has been studied as an alternative to steam-assisted gravity drainage (SAGD). This research presents a semi-analytical method for comparing oil drainage rates of SAGD and coinjection processes using different single-component solvents for a given set of reservoir/operating conditions. The oil recovery in coinjection involves complex interaction of energy and mass balances with the effects of gravity, phase behavior, and multiphase flow. We simplify the complex interaction without loss of fundamental mechanisms, while retaining the phase behavior details near the chamber edge.

The new method begins with solution for thermodynamic conditions at the chamber edge, where the phase transition occurs between two and three phases. Three components are considered; oil, solvent, and water. The chamber-edge conditions that are solved for are used to estimate distributions of solvent and temperature beyond the chamber edge. Darcy's law and material balance are then applied to derive an analytical expression for oil-drainage ratio, the ratio of oil drainage in coinjection to that in SAGD. Since the chamber-edge temperature and composition are interdependent for this ternary phase behavior problem, oil-drainage ratio is solved for as a function of solvent concentration in the oleic (L) phase at the chamber edge (x_{sL}^{edge}).

Case studies with the semi-analytical method show that oil-drainage ratio is higher in the higher x_{sL}^{edge} range than in the lower x_{sL}^{edge} range for a given coinjection solvent. This indicates that efficient oil recovery in coinjection requires high accumulation of solvent at the chamber edge. Oil-drainage ratios calculated for different coinjection solvents are compared in the high x_{sL}^{edge} range for preliminary screening of single-component coinjection solvents. This offers significant time savings in selecting a coinjection solvent by reducing the need for numerical reservoir simulation. The semi-analytical method also indicates that highly volatile solvents, which are relatively less expensive in general, tend to be more effective for less viscous reservoir oil and higher operating pressure. Less volatile solvents may offer more flexibility in operating conditions since they remain effective at lower pressures. These results are validated using fine-scale numerical reservoir simulations.

1. Introduction

Steam-assisted gravity drainage (SAGD) is the most widely commercialized process for bitumen and heavy-oil recovery in western Canada. In SAGD, the steam injected from a horizontal

* Corresponding author at: 3-114 Markin/CNRL Natural Resources Engineering Facility, University of Alberta, Edmonton, Alberta T6G 2W2, Canada. Tel.: +1 780 492 6121; fax: +1 780 492 0249.
E-mail address: rokuno@ualberta.ca (R. Okuno).
[1] Now at Schulich School of Engineering, University of Calgary, Canada.

http://dx.doi.org/10.1016/j.fuel.2014.12.030
0016-2361/

Nomenclature

A, B, C	viscosity correlation constants
a, b, c	K-value correlation constants
C	volumetric concentration in the L phase
C_3	propane
C_5	normal pentane
C_8	normal octane
g	gravitational acceleration
H	reservoir thickness above the producer
I_o	oil flow rate integral as defined by Eq. (13)
K	K value as defined by Eq. (6)
K_{ij}	K value as defined by Eq. (2)
k	permeability
k_r	relative permeability
L	oleic phase
MW	molecular weight
n	solvent distribution correlation constant
P	pressure
P_c	critical pressure
P_{inj}	injection pressure
P^{vap}	vapor pressure
q	volumetric flow rate
S	saturation
T	temperature
T_c	critical temperature
T_{crit}	critical temperature as defined in Section 3
T_R	Original reservoir temperature
T_R^*	upper limit of temperature in the integral of Eq. (13)
U_m	chamber propagation velocity at its top
V	gaseous phase
W	aqueous phase
x	mole fraction
x_{ij}	mole fraction of component i in phase j
z_i	overall composition of component i
α	thermal diffusivity of reservoir
α_c	compressibility
α_1	first thermal expansion coefficients
α_2	second thermal expansion coefficients
β	phase mole fraction
ε	empirical factor in temperature distribution profile
ρ	molar density
μ	viscosity
μ_{crit}	critical viscosity as defined in Section 3
Φ	porosity
ω	acentric factor
η	distance parallel to the chamber interface
ξ	distance perpendicular to the chamber interface

Subscripts and superscripts

edge	chamber edge
i	component index
j	phase index
L	oleic phase
N_p	phase index for the reference phase
o	oil component
ref	reference condition
res	residual
s	solvent component
V	vapor phase
w	water component
W	aqueous phase

Abbreviations

EOS	equation of state
RR	Rachford–Rice
SAGD	steam-assisted gravity drainage
SAP	solvent aided process
SOR	steam oil ratio
CSOR	cumulative steam oil ratio

well forms a steam chamber. The heated bitumen drains under gravity towards the production well located a few meters below the injection well [1].

High energy demand and environmental concerns associated with SAGD have entailed emerging alternative processes. Solvent–steam coinjection (referred to as coinjection) has been pilot-tested under different commercial names. In most of the coinjection processes, a small amount of hydrocarbon solvent is coinjected with steam to reduce further the viscosity of bitumen as a result of dilution in conjunction with heat. Successful applications of coinjection at the field and laboratory scales were reported in the literature. They improved oil production rates, ultimate recovery factors, and steam-oil ratio (SOR) in comparison with SAGD [2–11].

Besides promising results of coinjection tests, there are also reports showing that coinjection resulted in little improvement or even worse performance compared to SAGD [12–15]. Proper design is important for the practicality of coinjection processes [16].

Many studies have been conducted on the effects of solvent properties and concentration on various aspects of coinjection, such as oil production rate, ultimate recovery, and SOR [2,15,17–21]. These studies led to several proposals for optimum solvent selection and coinjection strategies. These results, however, are specific to the experimental conditions or reservoir properties considered [22]. They are sometimes contradictory to one another as described in Keshavarz et al. [23]. This implies that the effects of solvent selection and concentration on oil drainage in coinjection are not fully understood [22]. Interaction of energy and mass balances near the chamber edge is complicated even for coinjection of a single-component solvent [23].

A few analytical studies were conducted to better understand fundamental, macroscopic mechanisms involved in coinjection. Sharma and Gates [24] considered mathematical models to calculate the length scales of mass and heat transfer beyond the edge of a coinjection chamber. They defined two regions beyond the chamber edge. One is approximately 10 cm thick, where solvent mass transfer is dominant in oil viscosity reduction. The other is approximately 10 m thick, where heat transfer is dominant. They did not attempt to solve for a temperature and solvent concentration at the chamber edge in their calculations. Instead, the steam temperature at a chamber pressure and a certain solvent concentration were assumed at the chamber edge. The production rates calculated in their research are likely overestimated mainly because they did not consider the effect of solvent accumulation near the chamber edge on the temperature distribution beyond the edge [26,23].

Gupta and Gittins [22] developed a semi-analytical approach to estimate oil and solvent drainage in coinjection. Their mathematical model uses Butler's SAGD model [27,28] for heat effects on oil drainage, and a 1-D solvent mixing model for solvent distribution beyond the edge. They considered reduction of the chamber-edge temperature (T_{edge}) due to the existence of solvent, and solved for a solvent concentration at the chamber edge. The volatility of the reservoir oil was implicitly assumed to be zero.

Gupta and Gittins [22] had to make the effective diffusion coefficient three orders of magnitude greater than theoretical values available for bitumen/solvent systems in order to match field-observed results with their model. They gave an explanation for this inconsistency by considering significant oil drainage from inside the chamber in addition to that from beyond the chamber edge. However, the gas saturation is typically quite high in the chamber. It was not discussed in detail whether the oleic (L) phase mobility inside the chamber was sufficient to fill the gap between the field observations and calculations from their model. Butler [27,28] considered in his SAGD models no oil drainage inside the chamber, where the oil saturation is low.

The compositions at the chamber edge can be calculated as part of the thermodynamic conditions for the phase transition between L–W and V–L–W equilibria at a given temperature and pressure for a given fluid system [23,26]. V and W stand for the gaseous and aqueous phases, respectively. The solvent condensed at the chamber edge is mixed with reservoir oil components in the L phase. The reservoir mixing is caused by molecular diffusion and enhanced by spreading mechanisms with convection as discussed in Garmeh and Johns [29]. In coinjection with a SAGD well configuration, this convection is mainly the gravity drainage along the chamber edge. The transverse dispersion associated with the gravity drainage is likely the main driving force for spatial distribution of condensed solvent beyond the chamber edge. That is, at least two dimensions with gravity are required to model rigorously the mixing of solvent with oil components beyond the chamber edge.

Use of a 1-D solvent mixing model for calculating solvent distribution beyond the chamber edge in Gupta and Gittins [22] and Sharma and Gates [24] allows for neither a finite thickness of convection of the mobile L phase nor transverse dispersion in the L phase near the chamber edge. Since dispersion (i.e., enhanced mixing) does not occur without convection [29,30], their models can consider only diffusion beyond the chamber edge. This may be the fundamental reason for the inconsistency between model predictions and field observations in Gupta and Gittins [22].

Recently, Rabiei Faradonbeh et al. [25] have proposed a semi-analytical model to estimate the oil production rate during steam–solvent gravity drainage of heavy oil. Their model assumes a transient temperature and solvent distribution in the mobile liquid zone at the chamber edge. However, the temperature and solvent concentration at the chamber edge are constant in their model, and approximated by the steam–solvent system in the absence of bitumen. This is similar to the approach of Dong [26]. The occurrence of a significant temperature gradient inside the coinjection chamber can be largely explained using water–solvent binary mixtures as discussed in Dong [26] and Keshavarz et al. [23]. Keshavarz et al. [23] verified the effect of solvent on T_{edge} using numerical simulation, in which some simplifying assumptions made in Dong [26] were relaxed, such as the existence of the reservoir oil as a third component and fluids' non-idealities.

Keshavarz et al. [23,31] conducted a mechanistic simulation study of coinjection with a SAGD well pattern. They pointed out three main factors yielding increased oil production rate in coinjection; i.e., solvent accumulation, temperature distribution, and bitumen dilution with solvent near the chamber edge. They also explained how SAGD residual oil saturation can be further reduced via coinjection.

Keshavarz et al. [23] explained that an optimum volatility of solvent can be typically observed in terms of oil production rate for given operation conditions. The optimum volatility occurs as a result of the balance between two main factors affecting the L-phase mobility along the chamber edge; i.e., reduction of T_{edge} and superior oil dilution in coinjection of more volatile solvent. As the solvent becomes more volatile, T_{edge} tends to be lower and the solvent–bitumen mixing zone tends to be thinner. As the solvent becomes less volatile, the dilution effect becomes less. Therefore, a break-over point is typically observed on the average oil production rates with respect to solvent carbon number. They used this type of plots to find an optimum single-component solvent for given operation/reservoir conditions. The proposed procedure was also applied successfully to simulation case studies of Encana's solvent aided pilot (SAP) in Senlac and Nexen's expanding solvent-SAGD (ES-SAGD) pilot in Long Lake. However, this procedure requires numerical reservoir simulations for all coinjection solvents of interest, which can be quite time-consuming.

On the basis of these results from prior research, this paper presents a semi-analytical method for estimating an optimum single-component solvent in terms of oil production rate for given operating conditions. The method begins with solution for fluid properties at the chamber edge, where the phase transition occurs between the L–W and V–L–W equilibria. Three components are considered consisting of oil, solvent, and water. An inverted triangle is assumed as the chamber shape. Assumptions are also made for estimating distributions of temperature and solvent concentration beyond the chamber edge.

In prior numerical research [23,31], the primary mechanisms were speculated for oil production rate enhancement when solvent was coinjected with steam during SAGD. The semi-analytical model in this research confirms that the enhancement of oil production rate can be largely explained by the fundamental mechanics expressed semi-analytically. The presented method also enables to compare oil-drainage rates of coinjection processes with that of SAGD for a given set of operating/reservoir conditions. The method is validated using numerical reservoir simulations.

2. Theory

2.1. Solution for chamber-edge conditions

This section presents solution of thermodynamic relations for the phase transition between L–W and V–L–W equilibria at the chamber edge in coinjection of a single-component solvent and steam. The following assumptions are made: (1) ternary mixtures of water, a single-component solvent, and reservoir oil, (2) complete immiscibility between the W and L phases, (3) a negligible pressure gradient in the chamber, and (4) Raoult's law for phase equilibrium.

The water, oil, and solvent components are labeled with indices $i = w$, o, and s, respectively. The W, L, and V phases are expressed using indices $j = W$, L, and V, respectively. x_{ij} is the mole fraction of component i in phase j. Then, phase equilibrium for a ternary three-phase system at a given temperature (T) and pressure (P) is written as:

$$\begin{aligned} P_w^{vap} &= x_{wV}P \\ x_{oL}P_o^{vap} &= x_{oV}P \\ x_{sL}P_s^{vap} &= x_{sV}P \\ x_{oL} + x_{sL} &= 1.0 \\ x_{wV} + x_{oV} + x_{sV} &= 1.0. \end{aligned} \tag{1}$$

where P_i^{vap} is the vapor pressure of component i at T. The first equation is for the V–W equilibrium, the second and third equations for the V–L equilibrium, and the last two equations for summation constraints.

Partitioning of components between phases is expressed through K values defined as:

$$K_{ij} = \frac{x_{ij}}{x_{iN_P}} \tag{2}$$

where x_{iN_p} is the mole fraction of component i in a reference phase N_p. Once K values and an overall composition are given, the Rachford–Rice (RR) equations [36,37] are solved for phase mole fractions (β_j, $j = W, L$, and V);

$$f_j(\beta) = \sum_{i=w,o,s} \frac{(1-K_{ij})z_i}{1-\sum_{j=W,L}(1-K_{ij})\beta_j}$$
$$\sum_{j=W,L,V} \beta_j = 1.0. \quad (3)$$

After solving the RR equations for β_j, the equilibrium phase compositions are calculated as follows:

$$x_{iN_p} = \frac{z_i}{1-\sum_{j=W,L}(1-K_{ij})\beta_j}$$
$$x_{ij} = K_{ij}x_{iN_p}, (j \neq N_p) \quad (4)$$

A chamber edge in this study is defined where the phase transition between L–W and V–L–W occurs. That is, the overall composition at the chamber edge exists on the L–W edge of the V–L–W tie triangle at a given T and P, where the amount of the V phase is zero. This is schematically illustrated in composition space in Fig. 1.

Note that the W phase consists of 100% water, and the L phase does not contain the water component in this research. T_{edge} is the same for any overall composition on the L–W edge of the tie triangle. The solvent concentration on the water-free basis for possible overall compositions at the chamber edge at a given pressure and temperature is exactly the solvent concentration in the L phase for that tie triangle. Therefore, the solvent concentration in the L phase on the phase transition that occurs at the chamber edge is used as the composition information required for plotting chamber-edge temperatures in this research.

The solvent concentration in the L phase at the chamber edge is uniquely determined once P and T_{edge} are fixed, because a tie triangle is invariant in ternary composition space. Fig. 2 presents example calculation results for three different solvent components at 2000 kPa and 5000 kPa. This type of figures can be used to approximate the relationship between T_{edge} and x_{sL}^{edge} for a given pressure and solvent. Properties of the components used are listed in Table 1. The single-component representation of bitumen is taken from Mehrotra and Svrcek [34], which is based on the four-component representation of bitumen by Johnson [35].

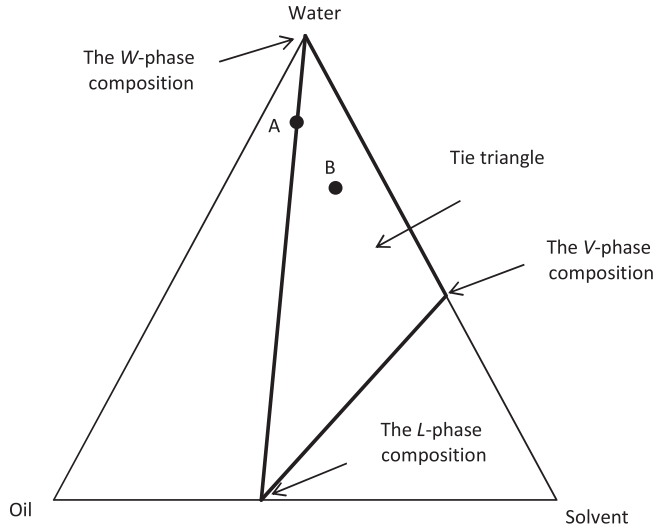

Fig. 1. Tie triangle for ternary mixtures of water, solvent, and oil at a given pressure and temperature. Overall composition A is on the W–L edge of the tie triangle and represents a condition at the chamber edge. Overall composition B is in the three-phase region and represents a condition inside the coinjection chamber.

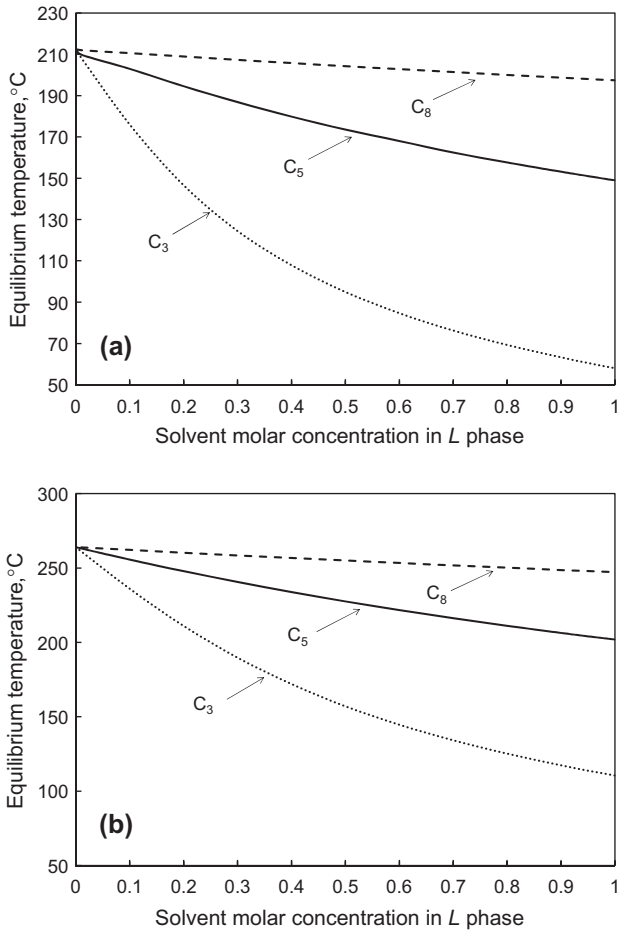

Fig. 2. Chamber-edge temperature with respect to solvent mole fraction in the L phase calculated for different solvents. (a) 2000 kPa and (b) 5000 kPa. Reservoir oil is an Athabasca-type bitumen with the properties listed in Table 1.

The K values of the water and solvent components are generated using the following correlation based on Raoult's law:

$$K_i(P,T) = \frac{P_i^{vap}}{P} = \frac{a}{P}e^{\frac{b}{T-c}}, \quad (5)$$

where P is the pressure in kPa and T is the temperature in °C. a, b, and c are the coefficients available in Reid et al. [38] and listed in Table 1. Due to the unavailability of these coefficients for the bitumen component, its vapor pressure was calculated by the Peng–Robinson (PR) equation of state [39]. The following transformation of variables should be considered before applying the K values in Eq. (5) to Eq. (3):

$$K_w = \frac{1}{K_{wW}},$$
$$K_o = \frac{1}{K_{oL}},$$
$$K_s = \frac{1}{K_{sV}}, \quad (6)$$

Fig. 2 presents that T_{edge} is lower for more volatile solvent for the same operating pressure and solvent concentration in the L phase. The two ends of the horizontal axis correspond to two limiting cases. At the left end, there is no solvent component present in the L phase as in SAGD, and the T_{edge} corresponds to

Table 1
Components' properties used in the chamber-edge temperature calculation.

Component	*MW* (kg/kg mol)	T_c (°C)	P_c (kPa)	ω	*a* (kPa)	*b* (°C)	*c* (°C)
Water	18	374.15	22088.850	0.344	1.1860×10^7	−3816.44	−227.02
C_3	44.1	96.65	4245.518	0.152	9.0085×10^5	−1872.46	−247.99
C_5	72.1	196.45	3374.120	0.251	1.0029×10^6	−2477.07	−233.21
C_8	114.2	295.65	2482.463	0.394	1.1187×10^6	−3120.29	−209.52
Oil	594.6	817.75	785.980	1.361	$K_o = \frac{P_o^{vap}}{P}$ where P_o^{vap} is calculated using the PR EOS		

the saturated steam temperature. Accumulation of solvent results in a reduction of T_{edge}. T_{edge} at the right end, where there is no bitumen component present, corresponds to the binary-mixture assumption of Dong [26].

Such accumulation of solvent can occur due to non-steady-state mass balance for solvent components near the chamber edge. That is, a volatile solvent tends to accumulate near the chamber edge when it tends to remain in the *V* phase, instead of condensing into the *L* phase that drains under gravity. To our knowledge, however, no closed-form solution has been presented for the composition variation along the chamber edge that results from multi-dimensional multi-phase non-isothermal flow inside and outside the chamber in coinjection processes. This is why the phase-transition temperature (as well as oil-drainage ratio presented in Section 2.3) is solved for as a function of composition in the current paper.

At certain stages of chamber propagation, the local *L* phase at the chamber edge may be composed of nearly 100% solvent. This can be beneficial in terms of displacement efficiency enhancement as discussed in Keshavarz et al. [23,31]. However, Fig. 2 shows that the reduction of T_{edge} can be quite significant depending on the level of solvent accumulation and the solvent component coinjected.

Partitioning of the solvent into the *L* phase occurs due to miscibility between hydrocarbon components. The transition from the *V*–*W*–*L* to *W*–*L* equilibrium occurs at a higher temperature compared to the transition from the *V*–*W* to *W*–*L* equilibria in binary mixtures of water and solvent. The latter transition corresponds to the lowest T_{edge} for each solvent in Fig. 2.

It is common practice to use a single component to represent bitumen in research on SAGD and coinjection processes [14,22,24,32,33]. Reliable characterization of bitumen/solvent/water interactions for coinjection processes has not been established in the literature. For example, it is unknown how many (pseudo) components are required to properly represent experimental phase behavior data, such as solubilities of solvents and water in bitumen and equilibrium phase densities/viscosities at a wide range of operating temperature and pressure. Therefore, this research uses the single-component representation of bitumen by Mehrotra and Svrcek [34], which has been used in the literature. This is also to exclude the effect of fluid characterization on conclusions of the current research, the main focus of which is on understanding of the primary mechanisms of bitumen production enhancement in coinjection processes. Use of a single component for bitumen also makes it simple to present the effect of solvent accumulation on T_{edge}, as shown in Fig. 2.

2.2. Approximate distributions of temperature and solvent beyond the chamber edge

Calculation of oil drainage beyond the chamber edge requires distributions of temperature and solvent between two boundaries; the chamber-edge conditions and the initial reservoir conditions. Analytical solution of energy and mass balances in coinjection, however, is challenging since it requires at least two dimensions with the effects of multiphase flow, gravity, and phase behavior. Therefore, conventional approximations are made to calculate distributions of temperature and solvent in this research.

As in Reis [40], an inverted triangle is assumed as the shape of the vertical cross section of the steam chamber, where the producer well is located at the bottom vertex. With this assumption, the chamber advance rate normal to the interface varies from zero at the bottom to a maximum, U_m, at the top.

The temperature profile as a result of steady-state conductive heat transfer ahead of the chamber can be written as:

$$\frac{T - T_R}{T_{edge} - T_R} = e^{\frac{-\varepsilon U_m \xi}{\alpha}}. \tag{7}$$

In Eq. (7), T_R is the original reservoir temperature, ξ is the perpendicular distance from the chamber edge, α is the thermal diffusivity of the reservoir material, and ε is an empirical constant. According to Reis [40], an ε value of 0.4 provides a reasonable match with experimental data. A value of 8×10^{-7} m^2/s is used for α in this research. A practical range for chamber advance rates is 1–15 cm/day, according to Gupta and Gittins [22]. As will be shown in the next section, however, the value used for U_m does not affect the semi-analytical solution for oil-drainage rates of coinjection processes in comparison with that of SAGD (oil-drainage ratios) in this research.

If the solvent–bitumen diffusion coefficients are constant in a 1-D solvent mixing model, solvent distribution beyond the chamber edge declines rapidly towards the original solvent concentration. However, the diffusion flux is considered to be inversely proportional to viscosity or viscosity to some power, and proportional to temperature or temperature to some power [24]. As a result, concentration profiles in diffusion experiments exhibited abrupt front-end profiles in Okazawa [41] and Oballa and Butler [42].

Due to the difficulty in analytical solution for 2-D solvent distribution in coinjection as discussed above and in the introduction section, a simple 1-D approximation is used as follows:

$$C_{sL} = C_{sL}^{edge}\left(\frac{T - T_{crit}}{T_{edge} - T_{crit}}\right)^n, \tag{8}$$

where C_{sL} is the solvent concentration in the *L* phase on a volumetric basis. C_{sL} is related to the molar concentrations as:

$$C_{SL} = \frac{\left(\frac{x_{sL}}{\rho_s}\right)}{\left(\frac{x_{sL}}{\rho_s} + \frac{x_{oL}}{\rho_o}\right)}, \tag{9}$$

where ρ_s and ρ_o are the molar densities of the solvent and bitumen components, respectively. *n* in Eq. (8) is a factor that determines the shape of profile. If *n* is smaller than unity, the resulting profile is concave with a front temperature T_{crit}. The value of *n* used in all coinjection cases in this research is 0.25. The resulting distribution shape is in agreement with the experimental observations by Okazawa [41] and Oballa and Butler [42] and the numerical simulation results in this research and Keshavarz et al. [23].

In Eq. (8), T_{crit} is the critical temperature below which the mixing between solvent and bitumen is negligible in the *L* phase. T_{crit} is related to the *L*-phase viscosity since the dispersive flux of components in the transverse direction from the chamber edge

requires the L-phase drainage along the edge. For a given T_{edge}, T_{crit} is calculated as the temperature that yields the μ_{crit} value through a specified bitumen viscosity–temperature relationship, where μ_{crit} is related to T_{edge} as:

$$\ln(\ln(\mu_{crit})) = -0.002T_{edge} + 2.196, \quad (10)$$

where viscosity and temperature are in cp and °C, respectively. In the absence of experimental data, Eq. (10) was obtained from numerical simulation results in this research as shown in Fig. 3. Data points in this figure were extracted from randomly-selected rows of the numerical reservoir model at randomly-selected time steps. μ_{crit} was determined as the bitumen viscosity at the average temperature of the two adjacent grid blocks between which the solvent concentration front exists. According to Fig. 3, μ_{crit} slightly decreases with increasing T_{edge}; the reduction is a few centipoises over the temperature change of 200 °C.

Eq. (8) gives an explicit relationship between T and C_s, which enables us to proceed in the derivation for the oil-drainage ratio between coinjection and SAGD. More rigorous estimation of solvent distribution beyond the chamber edge is an important issue to be resolved as shown in Gupta and Gittins [22]. However, this is beyond the scope of this research.

2.3. Oil-drainage ratio between coinjection and SAGD

This section presents a semi-analytical method for estimating oil-drainage ratio, which is defined as oil-drainage rate of a steam–solvent coinjection in comparison with that of SAGD. In this research, only single-component solvents are considered as coinjectants. Since the chamber-edge temperature and composition are interdependent for this ternary phase behavior problem, oil-drainage ratio is solved for as a function of solvent concentration in the L phase at the chamber edge (x_{sL}^{edge}).

Combining Darcy's law with material balance results in

$$q_o = \sqrt{0.5kk_{rL}g\phi\Delta S_o H(U_m \cdot I_o)}. \quad (11)$$

A derivation of Eq. (11) is presented in Appendix A. In this equation, q_o is the volumetric drainage rate of the bitumen component per unit length of the horizontal section along one side of the chamber edge, k is the absolute permeability, k_{rL} is the average relative permeability to the L phase beyond the chamber edge, g is the gravitational acceleration, ϕ is the porosity, and H is the reservoir thickness above the producer. ΔS_o is the reduction in the local bitumen saturation; that is,

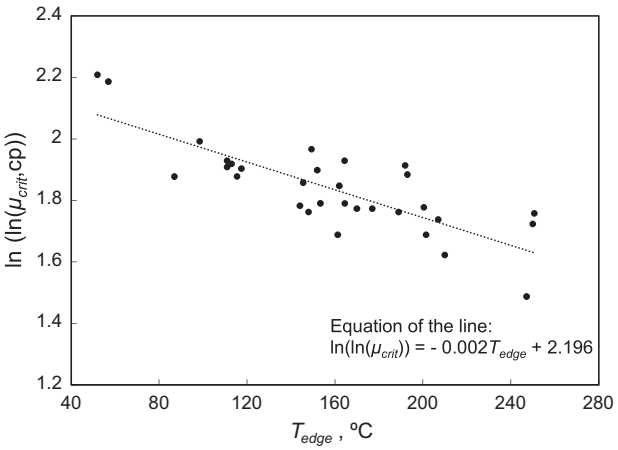

Fig. 3. Variation of μ_{crit} (cp) as defined in Section 3 with respect to T_{edge}. The scattered points were obtained from results of various numerical simulations in this research. The dashed line is the best fitted line for the data. The correlation, Eq. (10), is shown on the plot. μ_{crit} is in cp and T_{edge} is in °C.

$$\Delta S_o = S_{Li} - S_{Lres}^{edge} C_{oL}^{edge}, \quad (12)$$

where S_{Li} is the initial L-phase saturation, and S_{Lres}^{edge} is the residual saturation of the L phase at the chamber edge. C_{oL}^{edge} is the concentration of the bitumen component in the L phase at the chamber edge on a volumetric basis, which is calculated based on the chamber edge conditions (see Section 2).

The I_o parameter in Eq. (11) is an integral defined as below:

$$I_o = \int_0^{\infty} [(MW_L\rho_L C_{oL})/\mu_L]d\xi = -(\alpha/\varepsilon U_m)\int_{T_{edge}}^{T_R} \{[(MW_L\rho_L C_{oL})/\mu_L]/(T - T_R)\}dT, \quad (13)$$

where ρ_L, μ_L, and MW_L are the molar density, viscosity, and average molecular weight of the L phase, respectively. The second integral with respect to T can be obtained by transformation of variables using Eq. (7). Note that C_{oL} is 1.0 for SAGD.

The following mixing rules are used for the L-phase viscosity and density:

$$\mu_L = \exp[x_{oL}\ln(\mu_o) + x_{sL}\ln(\mu_s)] \quad (14)$$

$$\rho_L = [(x_{oL}/\rho_o) + (x_{sL}/\rho_s)]^{-1}, \quad (15)$$

where x_{sL} is the mole fraction of the solvent component in the L phase. μ_o and μ_s are the viscosities of the oil and solvent components, respectively. The following correlations are used to estimate the viscosity of the components as functions of temperature:

$$\ln(\mu_o(\text{cp})) = \exp(A + B\ln(T(K))), \quad (16)$$

$$\mu_s(\text{cp}) = A \cdot \exp(B/T(K)), \quad (17)$$

where A and B in Eq. (16) are given in Mehrotra and Svrcek [43] for Athabasca bitumen. A and B in Eq. (17) are given in Reid et al. [38]. The values used for the coefficients are listed in Table 2.

Molar densities of the oil and solvent components are modeled as functions of pressure and temperature through the following correlation:

$$\rho_i = \rho_{i,ref} \cdot \exp(\alpha_c(P - P_{ref}) - \alpha_1(T - T_{ref}) - 0.5\alpha_2(T^2 - T_{ref}^2)), \quad (18)$$

where P_{ref} is the reference pressure, T_{ref} is the reference temperature, and $\rho_{i,ref}$ is the reference molar density of component i. P_{ref} and T_{ref} are taken as 101.3 kPa and 15 °C, respectively. The values used for the α_c, α_1, and α_2 coefficients are given in Table 2.

According to Eq. (11), the oil-drainage ratio between coinjection and SAGD for a given reservoir can be written as:

$$q_{o,coinj}/q_{o,SAGD} = \sqrt{k_{rL,coinj}/k_{rL,SAGD}}\sqrt{\Delta S_{o,coinj}/\Delta S_{o,SAGD}} \times \sqrt{(U_m I_o)_{coinj}/(U_m I_o)_{SAGD}}. \quad (19)$$

The first term of the right-hand side of Eq. (19) is dependent on the saturation distributions beyond the chamber edge. Sharma and Gates [44] showed that oil saturation in the flowing-oil zone beyond the edge of a SAGD chamber ranges from the residual oil saturation at the chamber edge to the original oil saturation of the reservoir. In coinjection processes, the condensed solvent in the L phase beyond the chamber edge increases the L-phase saturation and thus the L-phase relative permeability, in comparison with SAGD. Keshavarz et al. [31] showed in their numerical simulations that saturation distributions in coinjection may be significantly different from those in SAGD. To our knowledge, however, no closed-form expression has been given in the literature for multiphase saturation distributions near the chamber edge in coinjection processes. Therefore, it is assumed in this research that the average relative permeability to the L phase beyond the chamber edge is fixed for SAGD and all coinjection cases (i.e., the first bracket on the right-hand side of Eq. (19) is unity). This may cause

Table 2
Oil and solvent components' properties used in calculation of I_o defined in Eq. (13).

Component	A	B	$\rho_{i,ref}$ (kg mol/m^3)	α_c, 1/kPa	α_1, 1/°C	α_2, 1/°C^2
C_3	0.021425	512.72	11.7234	2.54×10^{-6}	5.84×10^{-4}	3.41×10^{-6}
C_5	0.0191041	722.23	8.7360	1.69×10^{-6}	2.32×10^{-4}	2.82×10^{-6}
C_8	0.0131342	1090.70	6.1690	1.17×10^{-6}	1.02×10^{-4}	2.19×10^{-6}
Oil	22.851500	−3.57840	1.8060	3.24×10^{-7}	2.25×10^{-5}	6.31×10^{-7}

the oil drainage of a coinjection process to be underestimated in comparison with SAGD. If saturation distributions are known beyond the chamber edge, k_{rL} can be expressed as a function of ξ (or T) and be moved inside the integral of I_o defined by Eq. (13).

The second term on the right-hand side of Eq. (19) is slightly greater than 1.0. This is because C_{oL}^{edge} used in Eq. (12) is less than one for coinjection cases. This term captures the mechanism of improved displacement efficiency as a result of solvent coinjection with steam during SAGD, as discussed by Keshavarz et al. [31]. Values of S_{Li} and S_{Lres}^{edge} are 0.75 and 0.13 in this study.

It can be shown that the product of $(U_m I_o)$ in the third bracket on the right-hand side of Eq. (19) is independent of U_m with the equations used to estimate the distributions of properties beyond the chamber edge (see Appendix A). Thus, Eq. (19) can be rewritten as:

$$q_{o,coinj}/q_{o,SAGD} = \sqrt{\Delta S_{o,coinj}/\Delta S_{o,SAGD}}\sqrt{I_{o,coinj}/I_{o,SAGD}}, \quad (20)$$

for a fixed U_m. A value of 7 cm/day is used for U_m, although the value used does not affect calculation results.

The following steps are used for calculation of the oil-drainage ratio:

1. For a given P and solvent component, the system of phase equilibrium Eq. (1) is solved at temperatures ranging from the saturation temperature of pure water to the three-phase temperature of the water–solvent binary. x_{sL}^{edge} is obtained for each T_{edge}, resulting in a relationship between T_{edge} and x_{sL}^{edge} (see Fig. 2).
2. Temperature distribution beyond the chamber edge is calculated using Eq. (7).
3. Distributions of bitumen and solvent viscosities and densities, as a function of temperature beyond the chamber edge, are calculated using Eqs. (16)–(18).
4. Solvent distribution beyond the chamber edge is calculated using Eq. (8). μ_{crit} can be obtained using Eq. (10). T_{crit} can be obtained using μ_{crit} and Eq. (16). $C_s L^{edge}$ is related to x_{sL}^{edge} by Eq. (9).
5. Distributions of the L-phase viscosity and density are generated using the mixing rules given in Eqs. (14) and (15). The distribution of x_{sL} can be obtained by using Eq. (9) with the C_{sL} distribution from step 4 and the ρ_i distribution from step 3.
6. The first term of the right hand side of Eq. (20) is calculated with Eq. (12). The oil-drainage ratio is then evaluated numerically by replacing T_R in the upper limit of the integral in Eq. (13) with a sufficiently low value T_R^* (e.g., 20 °C). This can also be done by replacing ∞ in the upper limit of integral with the ξ value corresponding to T_R^*, if the integration is performed with respect to ξ.
7. Steps 2–6 are repeated for different values of x_{sL}^{edge} and the associated T_{edge}.

Different values are used for x_{sL}^{edge} in step 7 since we consider the interdependence between x_{sL}^{edge} and T_{edge}, and its effect on the oil drainage rate as presented in the next section. The two limiting cases are $x_{sL}^{edge} = 0$ and $x_{sL}^{edge} = 1$ corresponding to SAGD and Dong's binary consideration [26], respectively, as discussed before.

Semi-analytical solution is used because numerical evaluation of the integral is more efficient than analytical evaluation due to the complicated forms of ρ_L and μ_L as functions of ξ or T. The error associated with the numerical approach is small, considering that the integrand in Eq. (16) becomes negligible at a few meters in the cases considered in this research.

3. Sensitivity analysis

Previous sections presented a new semi-analytical method for estimating the oil drainage in single-component solvent coinjection, in comparison with that in SAGD, for a given reservoir. The calculation considered pressure, reservoir oil properties, and the interdependency between x_s^{edge} and T_{edge}. In this section, sensitivity analyses in terms of these parameters are presented through case studies.

3.1. Effect of solvent concentration at the chamber edge

This subsection presents a case study for coinjection of a single-component solvent for Athabasca bitumen at 2000 kPa. The main objective is to show how x_{sL}^{edge} affects the oil-drainage ratio for three different coinjection solvents, C_3, C_5, and C_8. Properties of fluid components are given in Tables 1 and 2. Other pertinent data for the calculation in this section are given in Table 3.

Fig. 4 presents the resulting oil-drainage ratios (see Eq. (20)) for three different coinjection solvents. The coinjection cases with C_5 and C_8 are similar to each other, and they both significantly improve the drainage rate compared to SAGD, as long as x_{sL}^{edge} (i.e., solvent accumulation at the chamber edge) is sufficiently high.

Coinjection of C_3 with steam does not result in significant improvement in oil-drainage rate for this case. It even deteriorates oil-drainage rate compared to SAGD for a wide range of x_{sL}^{edge}. This is mainly because T_{edge} rapidly decreases with x_{sL}^{edge} for the C_3 case as shown in Fig. 2. Temperature beyond the chamber edge is considerably lower than that of SAGD especially for high x_{sL}^{edge}. For $x_{sL}^{edge} < 0.60$, solvent accumulation is insufficient for the dilution effect to compensate the effect of the lowered temperature distribution on the L-phase viscosity. For $0.60 < x_{sL}^{edge} < 0.90$, the diluting effect of C_3 overtakes the effect of lowered temperature. The maximum improvement occurs approximately at $x_{sL}^{edge} = 0.80$. For $x_{sL}^{edge} > 0.80$, such a high concentration of C_3 at the chamber edge yields more than 125 °C temperature drop at the chamber edge in comparison with SAGD. This lowered temperature results in substantially high viscosity of the L phase, which limits the sol-

Table 3
Additional data needed for calculations of the oil-drainage ratio (as defined in Section 4) using the semi-analytical method.

Properties	Values
Initial L phase saturation	0.75
Residual L phase saturation	0.13
Initial reservoir temperature (°C)	13
Thermal diffusivity of the reservoir (m^2/s)	8×10^{-7}
T^* (°C)	20

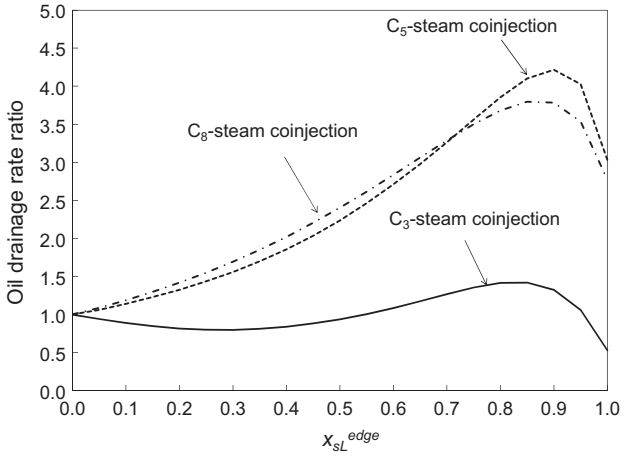

Fig. 4. The oil-drainage ratio as defined by Eq. (20) with respect to the solvent concentration in the L phase at the chamber edge (x_{sL}^{edge}). The operation pressure is 2000 kPa, and the oil is a typical Athabasca bitumen.

vent-mixing zone beyond the chamber edge. For $x_{sL}^{edge} > 0.90$, the region of solvent–bitumen mixing beyond the chamber edge is so thin that the overall effect of solvent dilution and temperature reduction is a production rate that is lower than in SAGD.

Fig. 5a presents the profiles of the integrand in Eq. (13) for SAGD and C_3 coinjection for various values of x_{sL}^{edge}. The area under each curve corresponds to I_o given in Eq. (13). Fig. 5b presents the profile of $\sqrt{\Delta S_{o,coinj}/\Delta S_{o,SAGD}}$ as a function of x_{sL}^{edge} when C_3 is coinjected with steam. This term increases with x_s^{edge} since the amount of the residual bitumen component at the chamber edge (i.e., $S_{Lr}^{edge} C_{oL}^{edge}$) decreases with increasing x_{sL}^{edge}. This is because a greater portion of the bitumen content in the residual L phase at the chamber edge is replaced by solvent as x_{sL}^{edge} increases. Note that ΔS_o is 0.62 for SAGD (i.e., $\Delta S_o = S_{Li} - S_{Lr}^{edge} = 0.62$) based on the assumptions made.

The effect of lowered T_{edge} is not severe for the C_5 and C_8 cases as shown in Fig. 2. The diluting effect can overtake the effect of lowered T_{edge} on the L-phase viscosity, regardless of x_{sL}^{edge}. However, the dilution becomes less effective for less volatile solvent for a given set of thermodynamic conditions. This is why C_5 coinjection exhibits higher oil-drainage ratios than C_8 coinjection when x_{sL}^{edge} is higher than approximately 0.70 in Fig. 4. As an example, Fig. 6 shows the distributions of temperature, solvent concentration, and the integrand in Eq. (13) for $x_{sL}^{edge} = 0.90$ for the C_5 and C_8 cases. Although the T_{edge} and solvent mixing zone are greater for the C_8 case, the drainage ratio (defined by Eq. (20)) is smaller for the C_8 case at this x_{sL}^{edge} value.

Results for the three coinjection cases show that the oil-drainage ratio is higher in the higher x_{sL}^{edge} range than in the lower x_{sL}^{edge} range. This is true also for different operating pressures and viscosity–temperature relations as presented in the subsequent subsections. It is important to properly represent thermodynamic conditions at the chamber edge, where the phase transition between L–V–W and L–V occurs. The simplistic assumption that T_{edge} is equal to the steam temperature at a given operating pressure, which was made in Sharma and Gates [24], will result in overestimation of oil-drainage rates in steam–solvent coinjection, especially for light coinjection solvents.

Plots of oil-drainage ratio in x_{sL}^{edge} space for different solvents (Fig. 4) can be used to estimate a range of solvent carbon numbers that are expected to result in higher oil-production rates than SAGD. For example, the oil-drainage ratios in the higher x_{sL}^{edge} range for different solvents in Fig. 4 indicate that C_3 is much worse than

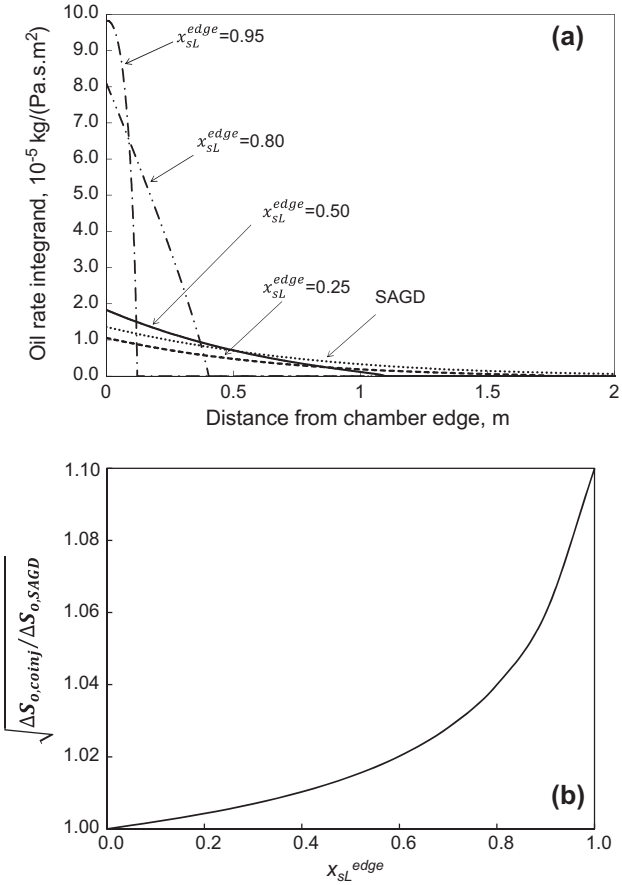

Fig. 5. (a) Variation of the integrand of Eq. (13) with respect to the distance from the chamber edge for selected values of x_{sL}^{edge}. (b) Variation of $\sqrt{\Delta S_{o,coinj}/\Delta S_{o,SAGD}}$ with respect to x_{sL}^{edge}. The operation pressure is 2000 kPa, and the oil is a typical Athabasca bitumen. Properties of all components are listed in Tables 1 and 2. For $x_{sL}^{edge} < 0.65$ the dilution effect is not sufficient to compensate the effect of lowered temperature distribution on the L-phase viscosity beyond the chamber edge. For $x_{sL}^{edge} > 0.90$, the region of solvent–bitumen mixing beyond the chamber edge is so thin that the overall effect of solvent dilution and temperature reduction is a lower production rate in C_3-steam coinjection compared to SAGD. The maximum flow rate improvement is calculated to occur around $x_{sL}^{edge} = 0.80$.

C_5 and C_8, and that C_5 and C_8 are similar to each other. It is likely that enhancement of oil production rate by coinjection levels off somewhere between C_5 and C_8 in terms of the volatility of single-component solvent. This is consistent with results from the method of Keshavarz et al. [23] for selecting an optimal coinjection solvent (see the introduction section). Unlike the average oil-production rates calculated in Keshavarz et al. [23], however, the semi-analytical method presented in this paper does not require time-consuming simulation runs, while retaining key mechanisms for oil-production enhancement by coinjection.

3.2. Effect of operating pressure

The operating pressure directly affects T_{edge}, which in turn affects distribution of temperature, viscosity, density, and solvent beyond the chamber edge. The three coinjection cases presented in the previous subsection are considered at a higher operating pressure. All other input data remain the same as in the previous subsection.

Fig. 7 presents the oil-drainage ratios calculated for three coinjection cases at 5000 kPa. Comparison with Fig. 4 reveals that the oil-drainage rate of the C_3 coinjection case is substantially increased by increasing the operating pressure. This is because of

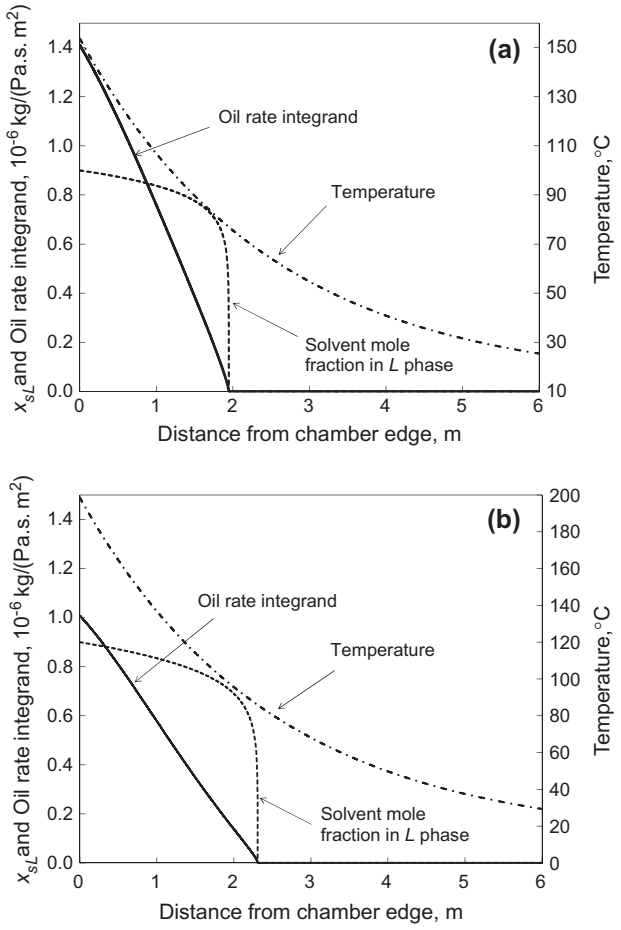

Fig. 6. Profiles of the integrand in Eq. (13), temperature, and solvent concentration in the L phase with respect to the distance from the chamber edge for $x_{sL}^{edge} = 0.90$. (a) C_5-steam coinjection and (b) C_8-steam coinjection. The higher temperature in the C_8 case results in a thicker solvent mixing zone compared to C_5. However, dilution is less effective with C_8. The overall effect is a greater area under the curve of the integrand for C_5-steam coinjection than C_8-steam coinjection.

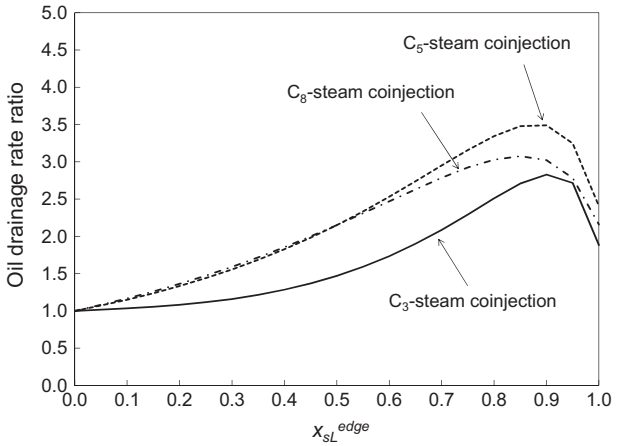

Fig. 7. The oil-drainage ratio as defined by Eq. (20) with respect to the solvent concentration in the L phase at the chamber edge (x_{sL}^{edge}). The operating pressure is 5000 kPa, and the oil is a typical Athabasca bitumen. Coinjection of highly volatile solvents (e.g., C_3) tends to be more efficient at higher operating pressure.

the exponential behavior of oil viscosity with respect to temperature. Increasing the operating pressure from 2000 kPa to 5000 kPa results in approximately 50 °C increase in the average T_{edge} for the coinjection cases studied here. The same amount of temperature increase yields much greater viscosity reduction at lower temperature; i.e., the temperature effect on viscosity is more significant in coinjection of more volatile solvent. Therefore, considerable improvement is observed in the mixing capability of more volatile solvent with bitumen beyond the chamber edge. All three coinjection cases show improved oil-drainage rates over SAGD in the entire range of x_{sL}^{edge} at 5000 kPa.

These results indicate that coinjection of highly volatile solvents, such as C_3, tends to be more efficient at higher operating pressures in terms of oil production rate. At a higher pressure, however, cumulative steam-to-oil ratio (CSOR) for a well-pair may be increased because (i) less latent heat is available per unit mass of steam, (ii) a larger amount of steam is required to occupy the V phase in the chamber, and (iii) a larger temperature difference between the chamber and surroundings causes faster heat conduction to the over- and under-burden. A detailed economic analysis should be conducted to evaluate quantitatively how much improvement is expected in oil production and additional costs associated with higher operating pressure.

As in the previous subsection, the C_5- and C_8-coinjection cases exhibit similar oil-drainage rates over a wide range of x_{sL}^{edge}. However, the effect of pressure is less significant for these two cases than for the C_3-coinjection case. This indicates that less volatile solvents may offer more flexibility in operating conditions for steam–solvent coinjection, which is important for a long-term operation that requires more careful implementation than SAGD.

3.3. Effect of oil viscosity behavior

Viscosity–temperature behavior of bitumen affects the mobility of the draining L phase and the thickness of the solvent mixing zone. Bitumen viscosity is typically in the range of 10^6 cp to 10^7 cp at initial reservoir conditions. Heavy oils show much lower viscosity on the order of 10^3 cp to 10^5 cp at the same temperature, but they are still too viscous for conventional recovery techniques. This section presents oil-drainage ratios calculated for a less viscous oil than Athabasca bitumen.

The oil viscosity used in this subsection is representative of Lloydminster heavy oil. The viscosity–temperature behavior of oil is taken from Hosseininejad et al. [45], and is given in Table 4. All other input data remain the same as those in Sections 2 and 3.1.

Fig. 8 presents the resulting oil-drainage ratios of the three coinjection cases. The C_5 and C_8 cases are similar to each other, and calculated to be more promising than the C_3 case in terms of oil production rate. Comparison of Figs. 8 and 4 indicates that the C_3 coinjection tends to be more effective for less viscous oil. The oil-drainage ratios of the C_3 case are above unity for the higher x_{sL}^{edge} range, and comparable to those of C_5- and C_8-coinjection cases for $x_{sL}^{edge} > 0.85$. This is because viscosity is less sensitive to temperature for heavy oil than for bitumen. However, if the concentration of C_3 at the chamber edge is low ($x_{sL}^{edge} < 0.4$ in Fig. 8), the diluting effect cannot compensate the effect of the lowered temperature distribution on the L-phase viscosity beyond the chamber edge.

4. Validation of the semi-analytical solution

The previous sections showed oil-drainage rates for the C_3-, C_5-, and C_8-coinjection cases in comparison with that for SAGD in x_{sL}^{edge} space. Results indicated that the C_5 and C_8 cases would give much higher oil production rate than the C_3 case and SAGD if sufficiently high x_{sL}^{edge} is achieved. In this section, these results from the semi-analytical method are validated against results from fine-scale numerical simulations using CMG's thermal reservoir simulator STARS [46].

Table 4
Viscosity–temperature for Lloydminster heavy oil.

Temperature (°C)	Viscosity (cp)
19.53	5201.51
29.33	2175.88
39.61	1004.96
49.40	428.80
59.67	227.50
69.45	133.27
79.72	75.04
89.97	50.49
99.74	33.31
109.51	24.26
119.28	17.67
130.02	13.13
139.78	10.56
150.03	8.16
160.27	6.83
170.03	5.60
179.79	4.88
189.55	4.16
200.28	3.62
209.55	3.15
219.79	2.75
230.03	2.54
239.80	2.00
250.04	1.78
259.31	1.61
270.03	1.49
279.79	1.40
299.78	1.24

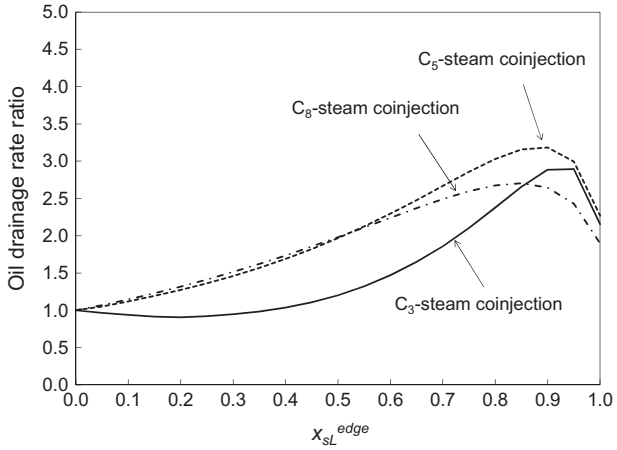

Fig. 8. The oil-drainage ratio as defined by Eq. (20) with respect to the solvent concentration in the L phase at the chamber edge (x_{sL}^{edge}). The operating pressure is 2000 kPa. The reservoir oil is less viscous than Athabasca bitumen with viscosity–temperature behavior given in Table 4. Comparison of Fig. 4 indicates that the C_3 coinjection tends to be more effective for less viscous oil.

A 2-D homogeneous reservoir with gravity is considered. The well-pair spacing, horizontal well length, and the reservoir thickness are 100 m, 500 m, and 20 m, respectively. The dimensions of the uniform grid block used are 0.5 m × 500 m × 1.0 m in the x, y and z directions, respectively. Simulation results were confirmed to be insensitive to further grid refinement. The injector and producer are located at the left boundary at the depths of 16 m and 20 m from the top, respectively. Thus, simulations are performed for a half of the chamber. The reservoir properties used are presented in Table 5. The relative permeability curves used are shown in Fig. 9. Capillarity and asphaltene precipitation are not considered. Dispersion is caused only by numerical dispersion in a fully implicit scheme with the single-point upstream weighting; physical diffusion/dispersion is not used in the simulations.

Table 5
Input data for the numerical simulations in Section 6.

Properties	Values
Porosity	0.33
Horizontal permeability	4000 md
Vertical permeability	3000 md
Initial reservoir pressure at depth of 500 m – Cases 1 and 3	1500 kPa
Initial reservoir pressure at depth of 500 m – Case 2	4500 kPa
Initial reservoir temperature	13 °C
Initial oil saturation	0.75
Initial water saturation	0.25
Formation compressibility	1.8E−5 1/kPa
Rock heat capacity	2600 kJ/m^3 °C
Rock thermal conductivity	660 kJ/m day °C
Over/underburden heat capacity	2600 kJ/m^3 °C
Over/underburden thermal conductivity	660 kJ/m day °C
Bitumen thermal conductivity	11.5 kJ/ m day °C
Gas thermal conductivity	2.89 kJ/ m day °C
Water thermal conductivity	50.1 kJ/ m day °C

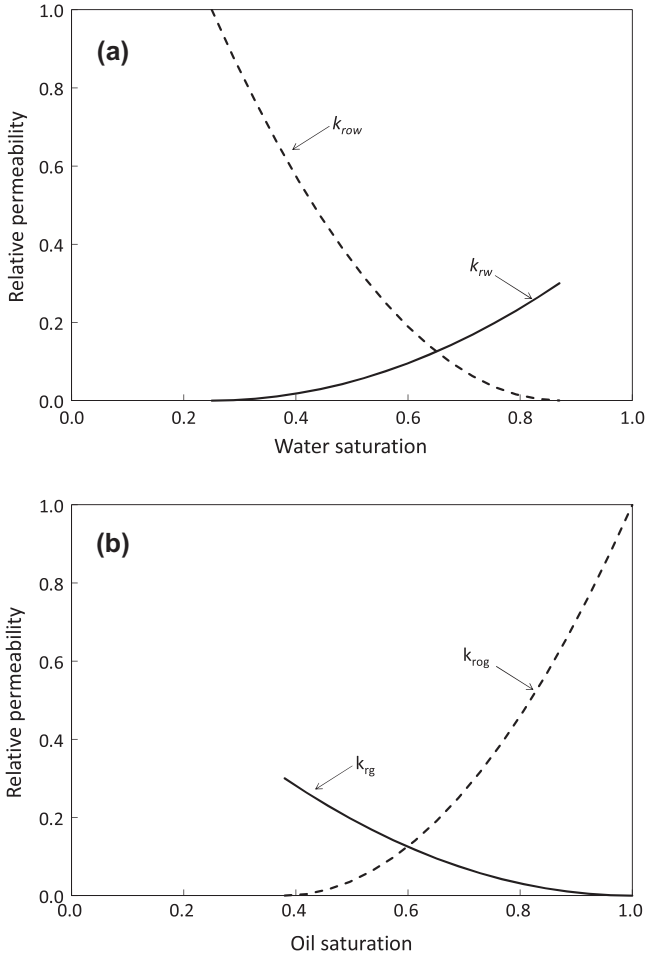

Fig. 9. Relative permeability curves used in the simulation cases (Section 6). (a) The water–oil system and (b) the liquid–gas system.

Three cases are considered for SAGD and different single-component-solvent coinjections as follows:

Case 1 (base case): SAGD/coinjection at an operating pressure of 2000 kPa for an Athabasca bitumen. Oil properties are given in Tables 1 and 2.

Case 2: SAGD/coinjection at an operating pressure of 5000 kPa for an Athabasca bitumen. Oil properties are given in Tables 1 and 2.
Case 3: SAGD/coinjection at an operating pressure of 2000 kPa for a less viscous oil than the Athabasca bitumen. Oil properties are the same as those in Tables 1 and 2 except for the viscosity–temperature behavior, which is presented in Table 4.

The producer is operated at a constant bottom hole pressure of 1500 kPa in Cases 1 and 3 and 4500 kPa in Case 2. Also, a maximum flow rate of 1.0 m^3/day is assigned to steam at the production well to prevent steam losses from the chamber. A quality of 90% is assigned to the injected steam at sandface. The solvent concentration in the injectant is 2.0 mol% in all coinjection simulations. Preheating of the reservoir is performed for six months. Properties of the solvent and water components in all simulation cases are given in Tables 1 and 2.

Fig. 10 presents bitumen production rates for the base case. According to the simulation results for the base case, the x_{sL}^{edge} ranges for the C_3, C_5, and C_8 cases are approximately [0.95, 1.00], [0.55, 0.85], and [0.60, 0.70] during the lateral expansion of chamber, respectively. Fig. 11 presents the average oil-drainage ratios simulated for the C_3, C_5, and C_8 cases during the lateral chamber expansion. The solvent portion of the produced L phase is excluded from the reported oil-production rates. Comparison with Fig. 4 indicates that the results from the semi-analytical model are in reasonable agreement with the numerical simulation results. This confirms that the presented model is capable of capturing the key mechanisms affecting oil drainage in steam–solvent coinjection with a SAGD well configuration.

As expected from the semi-analytical calculations in Fig. 4, the C_3 coinjection deteriorated the oil production rate compared to SAGD. This is because a significant accumulation of solvent at the edge of chamber lowers the temperature at the chamber edge. The C_5 and C_8 coinjection cases exhibit similar average production rates. They both resulted in significant improvements of oil production rate compared to SAGD.

Figs. 12 and 13 present the average oil-drainage rates simulated for Cases 2 and 3, respectively. Results from numerical simulations are in reasonable agreement with Figs. 7 and 8; i.e., unlike in the base case, the C_3 coinjection in Cases 2 and 3 results in improved oil production rates compared to SAGD. This was predicted by the semi-analytical method for Case 2, regardless of the solvent accumulation at the chamber edge. For Case 3, however, solvent accumulation resulting in $x_{sL}^{edge} > 0.4$ was required for C_3

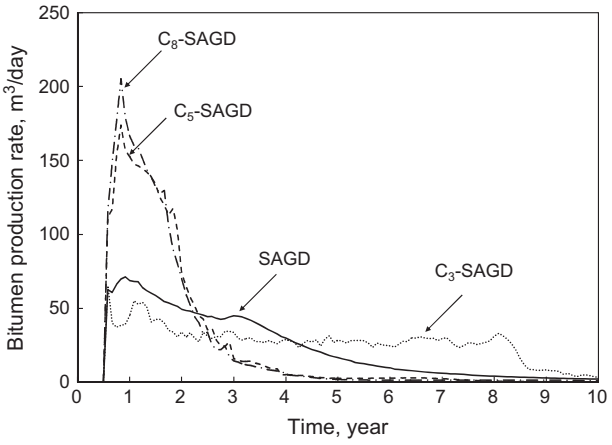

Fig. 10. Bitumen production rates for SAGD and three coinjection cases at 2000 kPa. The reservoir oil is an Athabasca bitumen. The solvent produced as part of the produced fluid in coinjection has been excluded.

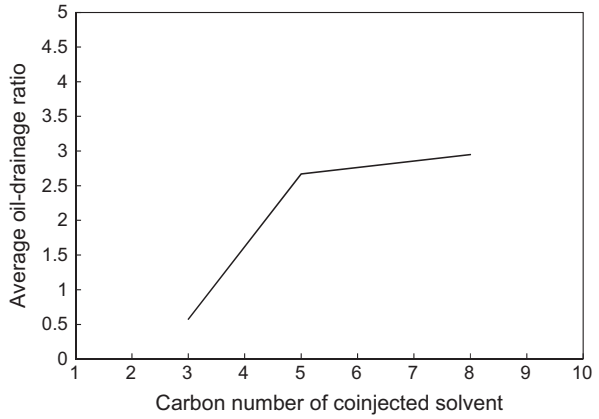

Fig. 11. Average oil-drainage ratios as defined by Eq. (20) during lateral chamber expansion for the base simulation case. Three solvent–steam coinjection processes are considered. The solvent produced as part of the produced fluid in coinjection has been excluded. The C_5 and C_8 cases results in improved oil-drainage rates. The C_3-steam coinjection deteriorates the oil-drainage rate compared to SAGD.

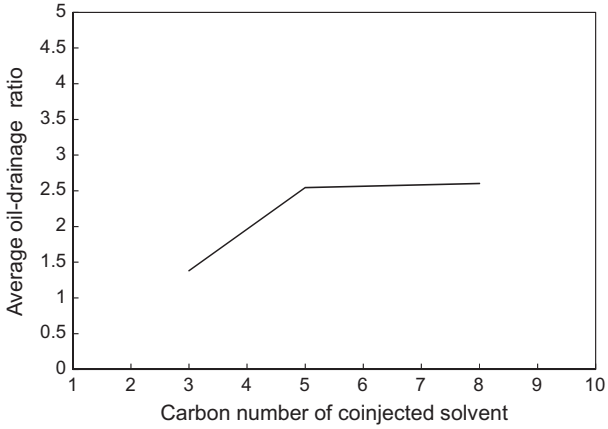

Fig. 12. Average oil-drainage ratios as defined by Eq. (20) during lateral chamber expansion for the simulation Case 2. Three solvent–steam coinjection processes are considered. The solvent produced as part of the produced fluid in coinjection has been excluded. Unlike in the base case, all the solvent–steam coinjection cases studied result in improved oil-drainage rate compared to SAGD.

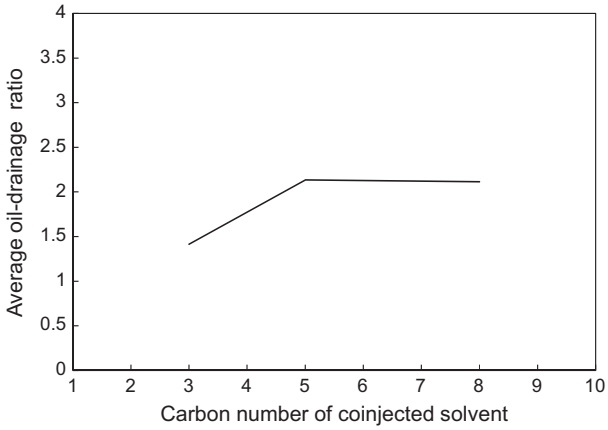

Fig. 13. Average oil-drainage ratios as defined by Eq. (20) during lateral chamber expansion for the simulation Case 3. Three solvent–steam coinjection processes are considered. The solvent produced as part of the produced fluid in coinjection has been excluded. As expected by the analytical solution, all the coinjection cases studied result in improved oil-drainage rate compared to SAGD.

Table 6
Comparison of the oil-drainage ratios predicted by the semi-analytical model and those obtained from numerical simulations.

Process	Reservoir oil viscosity	Operating pressure (kPa)	Average x_s^{edge}	Oil-drainage ratio from the semi-analytical model	Oil-drainage ratio from numerical simulations
C_3-SAGD	Athabasca-like	2000	0.95–1.00	0.53–1.06	0.57
C_5-SAGD	Athabasca-like	2000	0.55–0.85	2.46–4.10	2.67
C_8-SAGD	Athabasca-like	2000	0.60–0.70	2.83–3.29	2.95
C_3-SAGD	Athabasca-like	5000	0.65–0.80	1.90–2.51	1.38
C_5-SAGD	Athabasca-like	5000	0.55–0.80	2.33–3.34	2.54
C_8-SAGD	Athabasca-like	5000	0.55–0.70	2.31–2.78	2.60
C_3-SAGD	Lloydminster-like	2000	0.65–0.80	1.65–2.38	1.41
C_5-SAGD	Lloydminster-like	2000	0.55–0.80	2.12–3.03	2.13
C_8-SAGD	Lloydminster-like	2000	0.55–0.70	2.11–2.49	2.11

coinjection to achieve a higher oil-drainage rate than SAGD, as shown in Fig. 8. This is consistent with the numerical simulation, where the average values of x_{sL}^{edge} are in the range from 0.65 to 0.80 within the time period considered. The C_5 and C_8 cases show similar average production rates, and they are considerably higher than that of SAGD as predicted from Fig. 8. The average x_{sL}^{edge} values for the C_5- and C_8-coinjection cases are similar to those reported for Case 1.

Table 6 summarizes the oil-drainage ratios from the semi-analytical model and those from the numerical simulations. The average values of x_{sL}^{edge} reported in the 4th column of the table are extracted from numerical simulations during lateral expansion of the chamber. Results in the 5th column are estimations from the semi-analytical method based on the corresponding values given in the 4th column. The results from the numerical simulations in the right-most column fall within the predicted ranges by the semi-analytical method, except for C_3-steam coinjections of Case 2 and Case 3. Main reasons for the deviations may include the difference in solvent distribution between numerical simulations and the semi-analytical method through Eqs. 1, 8 and 10.

5. Results and discussion

Figs. 4, 7 and 8 indicated that oil-drainage rate in steam–solvent coinjection is highly dependent on the accumulation of solvent at the chamber edge, x_{sL}^{edge}. The maximum oil-drainage rate was calculated to occur at a high x_{sL}^{edge} between 0.75 and 0.90 for the cases studied in this research. Solvent accumulation beyond the chamber edge occurs due to slower drainage of solvent from the mobilized L-phase zone than solvent condensation near the edge. Keshavarz et al. [23] successfully controlled the level of solvent accumulation near the chamber edge by using variable solvent concentration in the injectant in their simulations of coinjection field pilots.

As T_{edge} becomes lower, the L-phase mobility beyond the chamber edge becomes lower, which in turn reduces the level of transverse mixing between solvent and bitumen beyond the chamber edge. This was qualitatively confirmed in the numerical simulation of C_3 coinjection for the base case in the preceding section. x_{sL}^{edge} builds up to high values (i.e., $x_{sL}^{edge} > 0.9$) rapidly, due to the limited thickness of the solvent–bitumen mixing zone beyond the chamber edge (see Table 6 for simulated x_{sL}^{edge} ranges). Such high x_s^{edge} falls beyond the optimum indicated in Fig. 4, and has reduced the oil-drainage rate of C_3 coinjection below that of SAGD for the base case. This indicates that reducing the C_3 concentration in the injectant may improve the oil-drainage rate.

The simulated x_{sL}^{edge} ranges are relatively low for C_3 coinjection in Cases 2 and 3, and C_5- and C_8-coinjection for Cases 1 through 3 (see Table 6). This is because relatively high average T_{edge} in these cases allows for effective mixing of solvent and bitumen in a thicker region beyond the chamber edge. Using a higher solvent concentration in the injectant may further improve the oil-drainage rate for these cases.

Keshavarz et al. [23,31] showed that L-phase saturation can be below the residual saturation (S_{Lr}) in coinjection simulation when the L phase with a high solvent concentration splits into the L and V phases on the phase transition between V–L–W and L–W at the chamber edge. The range of $0.75 < x_{sL}^{edge} < 0.90$ in Figs. 4, 7 and 8 is sufficient to result in considerable reduction of the L-phase saturation below typical SAGD S_{Lr} values inside the chamber. Thus, a sufficiently high accumulation of solvent at the chamber edge is a requirement for enhancement of both oil production rate and displacement efficiency.

The results clarified the primary mechanisms for oil production rate enhancement when solvent is coinjected with steam during SAGD. Selection of an optimum solvent for a specific set of field application conditions will still require numerical reservoir simulation that can properly represent the phase behavior of bitumen/solvent/water mixtures and its interaction with non-isothermal reservoir flow under heterogeneity and gravity. This is partly because selection of an optimum solvent requires the knowledge of the compositional variation along the chamber edge that results from reservoir flow. The primary application of the semi-analytical method is to calculate whether or not solvent coinjection has a potential of improving oil production rate in comparison with SAGD. Oil rate improvement presented as a function of solvent accumulation at the chamber edge can be used for this purpose.

The focus of this work was on the improvement of bitumen production rate; neither steam-oil-ratio (SOR) nor the total rate of solvent and bitumen. The assumptions and simplifications used in this work (see Appendix B) enable to decouple the proposed primary mechanisms from many other complexities, such as heterogeneity, 3-D flow, the effect of well-bore hydraulics on injection profile along the well, transverse/longitudinal dispersion at varying temperature/pressure, convective heat transfer, relative permeability changes, absolute permeability changes, water dissolution in oil, emulsion flow, asphaltene precipitation/deposition, formation of the solvent-rich liquid phase in the mixing zone, time-dependent solvent concentration and injection pressure.

6. Conclusions

This paper presented a semi-analytical method for estimating oil production rates for steam–solvent coinjection processes with different single-component solvents, in comparison with that for SAGD, for given reservoir and operation conditions. The effects of solvent type, operating pressure, and oil viscosity were presented on the oil drainage using the semi-analytical method and fine-scale numerical simulations. Conclusions are as follows:

1. Analytical calculation of thermodynamic conditions at the chamber edge was presented using three components, oil, solvent, and water. The temperature and composition at the chamber edge are interdependent when more than two components

are used. The chamber-edge temperature is the saturated steam temperature at the operating pressure if there is no solvent component as in SAGD. Solvent volatility and accumulation tend to reduce the chamber-edge temperature.

2. The ratio of oil-drainage rate in coinjection to that in SAGD (oil-drainage ratio) is calculated in the semi-analytical method as a function of the solvent concentration in the L phase at the chamber edge (x_{sL}^{edge}). The oil-drainage ratios calculated for different coinjection solvents can be compared in the high x_{sL}^{edge} range for preliminary screening of single-component coinjection solvents. The method also gives better understating of the key factors affecting the oil drainage beyond the chamber edge as follows:
   - The oil-drainage rate depends mainly on the mobility of the L phase. In a given solvent–steam coinjection process, solvent accumulation up to an optimum amount improves the dilution efficiency. Further accumulation, however, may not be beneficial as it reduces the temperature and the thickness of the solvent-mixing zone beyond the chamber edge.
   - The oil drainage rate is typically higher in the higher x_{sL}^{edge} range than in the lower x_{sL}^{edge} range for a given coinjection solvent. High accumulation of solvent at the chamber edge can be achieved by a proper coinjection strategy as presented in our prior research.
   - Less volatile solvent results in a higher chamber-edge temperature and thicker solvent-mixing zone beyond the chamber edge for a fixed x_{sL}^{edge}. Less volatile solvents may offer more flexibility in operating conditions since they remain effective at lower pressures. However, the dilution becomes less effective for less volatile solvent. Thus, an optimum solvent volatility is expected to exist in terms of oil production rate when the above-mentioned factors take a balance.
3. A highly volatile solvent (e.g., C_3), which is relatively less expensive in general, is unlikely as the optimum solvent for an Athabasca-type bitumen at low operating pressures. Such highly volatile solvents tend to be more effective for higher operating pressure and less viscous reservoir oil.
4. Calculation results from the semi-analytical method were validated using fine-scale numerical simulations. The validation indicates that the oil-drainage ratios from the semi-analytical method are in reasonable agreement with those obtained from numerical simulations. Thus, the presented method can be used for preliminary screening for coinjection solvents and estimation of oil-drainage rate of coinjection in comparison with that of SAGD. The semi-analytical method is more efficient than running numerical simulations and reduces the need for numerical reservoir simulation of coinjection processes.

Conversion factors

atm × 1.013 250 E+05	=Pa
bar × 1.0 E+05	=Pa
bbl × 1.589 873 E−01	=m^3
cp × 1.0 E−03	=Pa s
ft × 3.048 E−01	=m
(°F − 32)/1.8	=°C
(°F + 459.67)/1.8	=K
psi × 6.894 757 E+00	=kPa

Acknowledgements

A partial support for this research was obtained from the third author's (TB) NSERC Industrial Research Chair in Unconventional Oil Recovery (industrial partners are Schlumberger, CNRL, SUNCOR, Petrobank, Sherritt Oil, APEX Eng., PEMEX, and Statoil). Ryosuke Okuno gratefully acknowledges a partial financial support from NSERC for this research (RGPIN 418266).

Appendix A. Derivation of Eq. (11)

The chamber shape in SAGD and coinjection processes is assumed to be an inverted triangle, where the producer well is located at the lower vertex. From material balance, the bitumen flow rate along one side of the chamber per unit well length is:

$$q_o = \frac{d}{dt}(0.5\phi\Delta S_o H W_s) = 0.5\phi\Delta S_o H \frac{d}{dt}(W_s) = 0.5\phi\Delta S_o H U_m / \sin\theta, \quad \text{(A-1)}$$

where W_s is one half of the chamber width (see Fig. A1). The other parameters were defined in the earlier sections of this paper. Darcy's law for gravity drainage of bitumen along the chamber edge can be written as:

$$q_o = \int_0^{q_o} dq_o = k k_{rL} g I_o \sin\theta, \quad \text{(A-2)}$$

where I_o is defined in Eq. (13). Substituting $\sin\theta$ from Eq. A-2 into Eq. A-1 results in

$$q_o = \sqrt{0.5 k k_{rL} g \phi \Delta S_o H (U_m I_o)}. \quad \text{(A-3)}$$

The temperature interval in the integral given by Eq. (13) can be divided into two intervals, and the product of U_m and I_o can be written as:

$$U_m I_o = -(\alpha/\varepsilon)\left[\int_{T_{edge}}^{T_{crit}} \{[(MW_L \rho_L C_{oL})/\mu_L]/(T - T_R)\} dT + \int_{T_{crit}}^{T_R} \{[(MW_L \rho_L)/\mu_L]/(T - T_R)\} dT\right]. \quad \text{(A-4)}$$

The second integral of the right-hand side of Eq. A-4 depends only on how ρ_l and μ_l vary with T for a given set of T_R and T_{crit}. The first integral has a similar set of variables, but it contains C_{oL}, which in reality depends on how reservoir flow (convection and diffusion/dispersion) and phase behavior interact with each other at varying temperature beyond the chamber edge. However, C_{oL} is represented as a function of T in this research once the n exponent is set in Eq. (8). Within this research, therefore, it is how ρ_L, μ_L, and C_{oL} vary with T that affects $U_m I_o$, instead of how U_m alters the temperature distribution through Eq. (7). Once the temperature dependency of these parameters is set, the product of $U_m I_o$ is independent of U_m.

Appendix B. Major assumptions and simplifications used in this research

This appendix provides a list of the major assumptions and simplifications made in this research. The following assumptions are made for phase equilibrium calculations:

- Ternary mixture of water, single component bitumen, and single component solvent.
- Local equilibrium along the chamber edge.
- No mutual solubility between water and hydrocarbon components.
- A negligible pressure gradient inside the chamber.
- Raoult's law for phase equilibrium.
- Three equilibrium phases (L, V and W) inside the chamber and two equilibrium phases (L and W) outside the chamber.

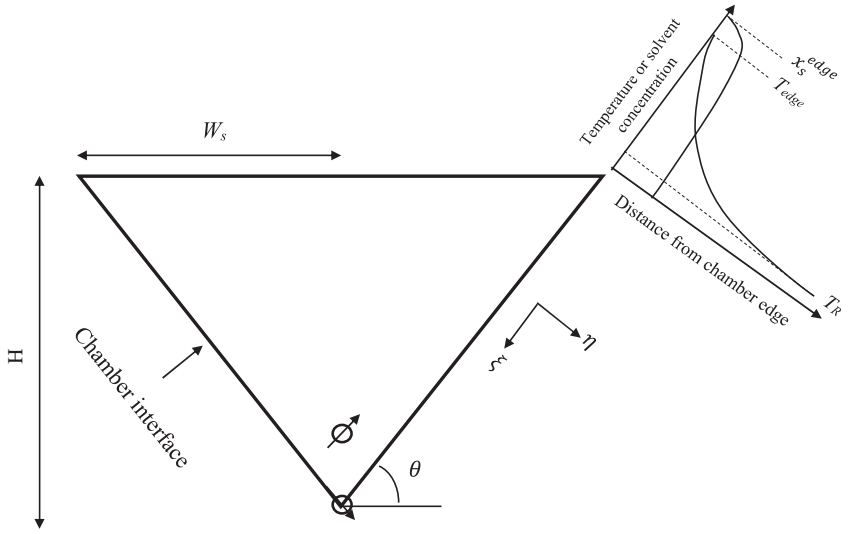

Fig. A1. Schematic of the 2-D cross section of the steam/steam–solvent chamber as an inverted triangle. The bottom vertex of triangle is attached to the production well. The chamber velocity normal to its interface varies from zero at the bottom to a maximum, U_m, at the top. Temperature and solvent distribution in the L phase beyond the chamber edge are also plotted against the distance from the chamber edge.

- No liquid–liquid separation of hydrocarbons.
- Negligible asphaltene precipitation.

The local equilibrium assumption is reasonable along the chamber edge, according to Edmunds [16]. He described that the vapor front would move only a few micro meters during the time required for equilibrium of a water/solvent/bitumen system.

The following major assumptions are made to approximate the solvent and temperature distribution beyond the chamber interface:

- Steam chamber has reached the top of the reservoir and is expanding laterally. An inverted triangle is assumed as the shape of the vertical cross section of the steam chamber, where the producer well is located at the bottom vertex (see Fig. A1). With this assumption, the chamber advance rate normal to the interface varies from zero at the bottom to a maximum, U_m, at the top.
- Heat transfer is only directed normal to the edge of the chamber. The heat transfer mechanism ahead of the chamber is assumed 1-D, steady-state and due to conduction only; i.e., the convection term is neglected.
- Uniform and constant thermal properties are assumed for the reservoir medium and fluids.
- A 1-D and simple approximation is used for solvent distribution as given by Eq. (8).

The following assumptions are made in the development of the Eq. (11) for oil production rate and Eq. (19) for oil drainage rate ratio:

- Darcy's law.
- Homogeneous and isotropic reservoir.
- Uniform and temperature- and composition-independent relative permeability curves.
- No variation in the rock, fluid and rock-fluid properties along the horizontal section of the wells.
- Identical fluids' saturation distributions ahead of the chamber edge for SAGD and all coinjection cases.

References

[1] Butler RM. Thermal recovery of oil and bitumen. Blackbook series. Calgary, Alberta: GravDrain Inc.; 1997.
[2] Nasr TN, Beaulieu G, Golbeck H, Heck G. Novel expanding solvent-SAGD process "ES-SAGD". J Can Petrol Technol 2003;42(1):13–6.
[3] Ivory J, Zheng R, Nasr T, Deng X, Beauulieu G, Heck G. Investigation of low pressure ES-SAGD. In: Paper SPE 117759 presented at 2008 SPE international thermal operations and heavy oil symposium, Calgary, Alberta, Canada, October 20–23, 2008.
[4] Gupta S, Gittins S, Picherack P. Field implementation of solvent aided process. J Can Petrol Technol 2005;44(11):8–13.
[5] Gupta S, Gittins SD. Christina lake solvent aided process pilot. J Can Petrol Technol 2006;45(9):15–8.
[6] Leaute RP. Liquid addition to steam for enhancing recovery of bitumen with CSS: evolution of technology from research concept to a field pilot at Cold Lake. SPE/Petroleum Society of CIM/CHOA Paper Number 79011, Calgary, Alberta, Canada, 4–7 November 2002.
[7] Leaute RP, Carey BS. Liquid addition to steam for enhancing recovery (LASER) of bitumen with CSS: results from the first pilot cycle. In: Paper number 2005–161 presented at the 56th Canadian international petroleum conference, Calgary, Alberta, Canada, 7–9 June 2005.
[8] Redford DA, McKay AS. Hydrocarbon-steam processes for recovery of bitumen from oil sands. In: Paper SPE 8823 presented at SPE/DOE enhanced oil recovery symposium, Tulsa, Oklahoma, USA, 20–23 April 1980.
[9] Li W, Mamora DD. Phase behavior of steam with solvent coinjection under steam assisted gravity drainage (SAGD) process. In: Paper SPE 130807 presented at the SPE EUROPEC/EAGE annual conference and exhibition, Barcelona, Spain, 14–17 June 2010.
[10] Ardali M, Barrufet M, Mamora DD. Laboratory testing of addition of solvents to steam to improve SAGD process. In: Paper SPE 146993 presented at SPE heavy oil conference Canada, Calgary, Alberta, Canada, 12–14 June 2012.
[11] Mohammadzadeh O, Rezaei N, Chatzis I. More insight into the pore-level physics of the solvent-aided SAGD (SA-SAGD) process for heavy oil and bitumen recovery. In: Paper SPE 157776 presented at SPE heavy oil conference Canada, Calgary, Alberta, Canada, 12–14 June 2012.
[12] Jiang Q, Butler R, Yee CT. The steam and gas push (SAGP)-2: mechanism analysis and physical model testing. In: Petroleum society's 49th annual technical meeting, Calgary, Alberta, Canada, 8–10 June 1998.
[13] Canbolat S, Akin S, Kovscek AR. A study of steam-assisted gravity drainage performance in the presence of noncondensable gases. In: Paper SPE 75130 presented at improved oil recovery symposium, Tulsa, Oklahoma, USA, 13–17 April 2002.
[14] Hosseininejad Mohebati M, Maini BB, Harding TG. Numerical evaluation of hydrocarbon additives to steam in the SAGD process. J Can Petrol Technol 2010;49(9):42–55.
[15] Li W, Mamora DD, Li Y. Solvent-type and -ratio impacts on solvent-aided SAGD process. SPE Reservoir Eval Eng 2011;14(3):320–31.
[16] Edmunds NR. Observations on the mechanisms of solvent-additive SAGD processes. In: Paper SPE 165419 presented at the SPE heavy oil conference Canada, Calgary, Alberta, Canada, 11–13 June 2013.
[17] Gupta SC, Gittins SD. Effect of solvent sequencing and other enhancements on solvent aided process. J Can Petrol Technol 2007;46(9):57–61.

[18] Govind PA, Das SK, Srinivasan S, Wheeler TJ. Expanding solvent SAGD in heavy oil reservoirs. In: Paper SPE/PS/CHOA presented at the 2008 SPE international thermal operations and heavy oil symposium, Calgary, Alberta, Canada, 20–23 October 2008.
[19] Gates ID, Gutek AMH. Process for in situ recovery of bitumen and heavy oil. U.S. Patent 7464756, 2008.
[20] Gates ID, Chakrabarty N. Design of steam and solvent injection strategy in expanding solvent steam-assisted gravity drainage. J Can Petrol Technol 2008;47(9):12–9.
[21] Jiang H, Deng X, Huang H, Beaulieu G, Heck G, Akinlade OG, Nasr TN. Study of solvent injection strategy in ES-SAGD process. In: Paper SPE 157838 presented at SPE heavy oil conference, Calgary, Alberta, Canada, 12–14 June 2012.
[22] Gupta S, Gittins SD. An investigation into optimal solvent use and the nature of vapor/liquid interface in solvent-aided SAGD process with a semianalytical approach. SPE J 2012;17(4):1255–64.
[23] Keshavarz M, Okuno R, Babadagli T. Optimal application conditions for steam-solvent coinjection. SPE Reservoir Eval Eng 2013; 28: 2014. doi: 10.2118/165471-PA.
[24] Sharma J, Gates ID. Steam–solvent coupling at the chamber edge in an in situ bitumen recovery process. In: Paper SPE 128045 presented at the SPE oil and gas India conference and exhibition, Mumbai, India, 20–22 January 2010.
[25] Rabiei Faradonbeh M, Harding TG, Abedi J. Semi analytical modelling of steam–solvent gravity drainage of heavy oil and bitumen, Part 2: unsteady-state model with curved interface. In: Paper SPE 170123-MS presented at the 2014 SPE heavy oil conference, Calgary, Alberta, Canada. 10–12 July 2014.
[26] Dong L. Effect of vapor-liquid phase behavior of steam-light hydrocarbon systems on steam assisted gravity drainage process for bitumen recovery. Fuel 2012;95:159–68.
[27] Butler RM. A new approach to modelling steam assisted gravity drainage. J Can Petrol Technol 1985;24(3):42–51.
[28] Butler RM. Steam-assisted gravity drainage: concept, development, performance and future. J Can Petrol Technol 1994;33(2):44–50.
[29] Garmeh G, Johns RT. Upscaling of miscible floods in heterogeneous reservoirs considering reservoir mixing. SPE Reservoir Eval Eng 2010;13(5):747–63. SPE-124000-PA.
[30] Adepoju OO, Lake LW, Johns RT. Investigation of anisotropic mixing in miscible displacements. SPE Reservoir Eval Eng 2013;16(1):85–96. SPE-159557-PA.
[31] Keshavarz M, Okuno R, Babadagli T. Efficient oil displacement near the chamber edge in ES-SAGD. J Petrol Sci Eng 2014;118:99–113.
[32] Jha RK, Kumar M, Benson I, Hanzlik E. New insights into steam/solvent-coinjection-process mechanism. SPE J 2013;18(5):867–77.
[33] Yazdani A, Alvestad J, Kjonsvik D, Gilje E, Kowalewski E. A parametric simulation study for solvent co-injection process in bitumen deposits. In: Paper SPE 148804 presented at the Canadian unconventional resources conference, Calgary, Alberta, Canada, 15–17 November 2011.
[34] Mehrotra AK, Svrcek WY. Corresponding states method for calculating bitumen viscosity. J Can Petrol Technol 1987;26(5):60–6.
[35] Johnson SE. Gas-free and gas-saturated bitumen viscosity prediction using the extended principe of corresponding states. M.Sc. thesis, University of Calgary, Calgary, Alberta, 1985.
[36] Rachford Jr. HH, Rice JD. Procedure for use of electronic digital computers in calculating flash vaporization hydrocarbon equilibrium (technical note 136). J Pet Tech 4 (10): 19. Trans, AIME, 195: 327–328. SPE-952327-G.
[37] Okuno R, Johns RT, Sepehrnoori K. A new algorithm for Rachford–Rice for multiphase compositional simulation. SPE J 2010;15(2):313–25. SPE-117752-PA.
[38] Reid RC, Prausnitz JM, Sherwood TK. The properties of gases and liquids. McGraw-Hill; 1977.
[39] Peng D-Y, Robinson DB. A new two-constant equation of state. Ind Eng Chem Fundam 1976;15(1):59–64.
[40] Reis JC. A steam-assisted gravity drainage model for tar sands: linear geometry. J Can Petrol Technol 1992;31(10):14–20.
[41] Okazawa T. Impact of concentration-dependence of diffusion coefficient on VAPEX drainage rates. J Can Petrol Technol 2009;48(2):47–54.
[42] Oballa V, Butler RM. An experimental study of diffusion in the bitumen-toluene system. J Can Petrol Technol 1989;28(2):63–9.
[43] Mehrotra AK, Svrcek WY. Viscosity of compressed Athabasca bitumen. Can J Chem Eng 1986;64(5):844–7.
[44] Sharma J, Gates ID. Multiphase flow at the edge of a steam chamber. Can J Chem Eng 2010;88(3):312–21.
[45] Hosseininejad Mohebati M, Maini BB, Harding TG. Numerical-simulation investigation of the effect of heavy-oil viscosity on the performance of hydrocarbon additives in SAGD. SPE Reservoir Eval Eng 2012;15(2):165–81. SPE-138151-PA.
[46] Computer Modelling Group (CMG) Ltd. STARS User Manual. Version 2012. Calgary, Alberta, Canada, 2012.